Surface modes and acoustic scattering of microspheres and ultrasound contrast agents

Omar Falou[a)]
Department of Electrical and Computer Engineering, Ryerson University, 350 Victoria Street, Toronto, Ontario, M5B 2K3, Canada

Amin Jafari Sojahrood, J. Carl Kumaradas, and Michael C. Kolios
Department of Physics, Ryerson University, 350 Victoria Street, Toronto, Ontario, M5B 2K3, Canada

(Received 8 August 2011; revised 10 July 2012; accepted 16 July 2012)

Surface modes of spherical objects subject to ultrasound excitation have been recently proposed to explain experimental measurements of scattering from microspheres and ultrasound contrast agents (UCAs). In this work, the relationship between surface modes and resonance frequencies of microspheres and UCAs is investigated. A finite-element model, built upon the fundamentals of wave propagation and structural mechanics, was introduced and validated against analytical solutions (error $<5\%$). Numerical results showed the existence of a systematic relationship between resonance frequencies and surface modes of a 30 μm microsphere driven at 1–70 MHz. On the contrary, for a 100 nm shelled, 4 μm diameter UCA, no clear relationship between the resonance frequencies and the surface modes was found in the frequency range examined. Instead, the UCA exhibited a collection of complex oscillations, which appear to be a combination of various surface modes and displacements. A study of the effects of varying the shell properties on the backscatter showed the presence of peaks in the backscatter of thick-shelled UCAs, which are not predicted by previous models. In summary, this work presents a systematic effort to examine scattering and surface modes from ultrasound contrast agents using finite-element models.
 [http://dx.doi.org/10.1121/1.4740505]

PACS number(s): 43.80.Qf, 43.20.Ks, 43.20.Fn [CCC] Pages: 1820–1829

I. INTRODUCTION

Ultrasound contrast agents (UCAs) are gas-filled, encapsulated bubbles that are administered intravenously to the venous system. They are very small (<8 μm), which enables them to pass through capillaries, but big enough so that they remain in the vasculature (Stride and Saffari, 2003). UCAs have a high degree of echogenicity, and hence they enable contrast between blood and the surrounding tissue (Greis, 2011). Depending on the contrast agent, the shell thickness can vary from a few nanometers to a few hundred nanometers and is composed of material such as polymers, albumin, phospholipids, and surfactants (Calliada *et al.*, 1998).

The first mathematical formulation that predicts the dynamic response of an air bubble (no shell) subject to a time-varying input pressure field is known as the Rayleigh–Plesset (RP) equation. The RP equation has several limitations. It is only applicable to a gas bubble oscillating in an incompressible fluid and can only predict the radially symmetric oscillations of the bubble; hence it cannot be used to model the behavior of UCAs that have an encapsulating shell (Leighton, 2004). The RP equation has been modified by many authors to take into account the presence of shell, which increases both the overall mechanical stiffness of the bubble and its acoustic damping. De Jong and Hoff (1993) modeled the behavior of UCAs by incorporating experimentally measured mechanical properties of the shell into the RP equation. Church (1995) derived a RP-like equation describing the dynamics of UCAs in which the shell is assumed to be a continuous layer of solid viscoelastic material. Allen *et al.* (2001) used modal series solution to shown that albumin-shelled contrast agents in the 1–40 MHz range support dipole resonance in addition to the monopole resonance predicted by other models (De Jong and Hoff, 1993; Church, 1995; Doinikov and Dayton, 2007).

Finite-element analysis combined with other numerical techniques, such as the boundary element method, infinite elements, and T-matrix method have been used in the past to model acoustic scattering from various objects submerged in a fluid (Hunt *et al.*, 1975; Wilton, 1978; Numrich *et al.*, 1981; Everstine and Henderson, 1990; Eaton and Regan, 1996). The near-field scattering was typically modeled using finite elements, while other techniques were used to find the far-field scattering. Most of these studies concentrated on scattering from rigid objects (Hunt *et al.*, 1975; Demkowicz and Shen, 2006). Recently, Falou *et al.* (2005, 2006a,b) developed a three-dimensional (3-D) finite-element model to study acoustic wave scattering from spherical objects and biological cells. Pauzin *et al.* (2007) used a similar model to investigate the changes in the monopole resonance frequency of various thick-shelled UCAs (in which the shell thickness is 10% of the UCA radius). Their model was based on the near-field calculations of the pressure field, which showed good agreement with analytical solutions (De Jong and Hoff, 1993; Church, 1995; Doinikov and Dayton, 2007).

a)Author to whom correspondence should be addressed. Electronic mail: ofalou@ryerson.ca

 0001-4966/2012/132(3)/1820/10/$30.00

Experimental studies were also conducted to investigate the dynamic response and backscatter of UCAs (Deng *et al.*, 1998; Moran *et al.*, 2002; Versluis *et al.*, 2004; Goertz *et al.*, 2005; Ketterling *et al.*, 2007; Dollet *et al.*, 2008). While some authors reported backscatter from UCAs centered at the transducer central frequency with no harmonic components (Deng *et al.*, 1998; Moran *et al.*, 2002), others observed the presence of harmonics in the backscatter of a lipid-shelled UCA, Definity™ (Bristol-Myers Squibb, North Billerica, MA) (Goertz *et al.*, 2005). Recently, Ketterling *et al.* (2007) reported the presence of subharmonics in the response of a polymer-shelled UCA, Point (POINT Biomedical, San Carlos, CA). In addition, non-spherical oscillations were observed for phospholipid shelled UCAs (Versluis *et al.*, 2004; Dollet *et al.*, 2008). Despite these theoretical and experimental efforts, the behavior of UCAs is not fully understood (Stride and Saffari, 2003). For instance, current analytical models do not incorporate shape oscillations or surface modes (Versluis *et al.*, 2004; Dollet *et al.*, 2008). These surface modes may alter the backscatter characteristics of these UCAs.

Surface modes are thought to occur as a result of the existence of surface waves (shell waves in the case of UCAs), which travel along the free surface of the scatterer. These modes are denoted by n, which is the number of wavelengths of the surface distortion that span the sphere's circumference (Uberall *et al.*, 1996). Basic surface modes include the breathing mode ($n=0$), where the sphere contracts and expands periodically (also known as radial or monopole oscillation). In the dipole mode ($n=1$), the sphere oscillates rigidly back and forth, whereas in the quadrupole mode ($n=2$), the shape alternates between a prolate and an oblate spheroid, etc. (Uberall *et al.*, 1996). Higher order surface modes exhibit more complex oscillations and displacements.

This work aims to investigate the use of finite-element models of wave propagation, coupled with stress–strain equations describing the interactions of the incident wave with either a solid sphere or a shelled spherical object. Model predictions are compared to available analytical solutions for elastic microspheres and the predicted resonances of UCA. Microspheres were chosen since analytical solutions for their backscatter responses were developed (Faran, 1951) and validated experimentally by previous investigators (Baddour *et al.*, 2005; Falou *et al.*, 2010).

We show how this model can also accurately predict the resonance frequencies of UCAs predicted by the Church model (Church, 1995). We use this framework to then investigate surface mode generation and to establish a relationship between UCA properties, resonance frequencies, and corresponding surface modes.

II. METHODS

In this work, we introduce a finite-element model to investigate the relationship between the far-field ultrasonic backscatter response of microspheres and UCAs and their corresponding non-spherical oscillations. The model describes the basic fundamentals of sound wave propagation using the Helmholtz equation in addition to the stress–strain relationship within elastic material and is capable of predicting the dynamic response of spherical objects, particularly surface modes. Briefly, designing and solving a problem using finite-element analysis involves the following steps: Geometry creation, defining material properties, and discretization of the computational domain into finite elements. Domain discretization involves the creation of a system of points called nodes, which makes a grid called a mesh. This is followed by defining boundary condition and the assembly of elements together while satisfying the requirements of equilibrium and continuity between them. The result of the assembly process is a set of algebraic equations represented in matrix form. The last step involves solving the resulting algebraic equations and interpreting the results. The COMSOL Multiphysics™ 3.5a (COMSOL, Inc., Burlington, MA) software package was used as a platform for the finite-element model development. A spherical geometry, such as that of polystyrene microspheres for which analytical solutions have been validated experimentally (Baddour *et al.*, 2005; Falou *et al.*, 2010), was chosen for the first stage of the model development, since analytical solutions exist that enable the comparison of computational and analytical results and hence allows for the validation of the developed finite-element model. The scatterer is located in the center of the computational domain with different acoustic properties than those of the surrounding fluid. The scatterer is insonified by a plane wave traveling in the $+z$ direction.

Due to the symmetric nature of the problem, the 3-D model can be simplified by a two-dimensional (2-D) axisymmetric model, with the z axis being the axis of the symmetry. The 2-D axisymmetric model requires less computational resources and execution times than 3-D models, particularly at high frequencies where more mesh elements are required as a result of the short ultrasonic wavelengths contained in the incident pulse.

A. Polystyrene microsphere

An example of a scatterer that supports both longitudinal and shear waves is polystyrene microspheres used for the calibration of cell counters. Baddour *et al.* (2005) and Falou *et al.* (2010) have shown good agreement between analytical solutions and experimental backscatter measurements of polystyrene microspheres suspended in water. The acoustic pressure p depends on the radial (r), axial (z), and azimuthal (φ) coordinates and is given by (Ihlenburg, 1998; COMSOL, Inc., 2008)

$$p(r,z,\phi) = p(r,z)e^{-im\phi}, \tag{1}$$

where m is the circumferential wave number. The time-harmonic Helmholtz wave equation was used to model propagation of sound waves in the domain outside the scatterer,

$$\frac{\partial}{\partial r}\left[\frac{r}{p}\left(\frac{\partial p}{\partial r}\right)\right]+r\frac{\partial}{\partial z}\left[\frac{1}{\rho}\left(\frac{\partial p}{\partial z}\right)\right]+\left[\left(\frac{\omega}{c}\right)^2-\left(\frac{m}{r}\right)^2\right]\frac{rp}{\rho}=0, \tag{2}$$

where p is the acoustic pressure, ρ is the mass density of the medium, ω is the angular frequency ($\omega=2\pi f$) of the wave, and c is the speed of the wave in the medium. The

surrounding medium was assumed to be water having a density and speed of sound of 1000 kg/m^3 and 1483 m/s, respectively. The constitutive equation for linear elastic material was used to describe the stress–strain relationship in the microsphere. The stress σ and the strain ε are related by Hooke's law for isotropic material (Oñate, 2009; Logan, 2012),

$$\sigma = [D]\varepsilon, \tag{3}$$

where $[D]$ is given by

$$[D] = \frac{E}{(1+\nu)(1-2\nu)} \begin{bmatrix} 1-\nu & \nu & \nu & 0 \\ \nu & 1-\nu & \nu & 0 \\ \nu & \nu & 1-\nu & 0 \\ 0 & 0 & 0 & \frac{1-2\nu}{2} \end{bmatrix}, \tag{4}$$

$$\sigma = \begin{pmatrix} \sigma_r \\ \sigma_z \\ \sigma_\phi \\ \tau_{rz} \end{pmatrix}, \tag{5}$$

and

$$\varepsilon = \begin{pmatrix} \varepsilon_r \\ \varepsilon_z \\ \varepsilon_\phi \\ \gamma_{rz} \end{pmatrix}. \tag{6}$$

E is the Young's modulus, ν is the Poisson's ratio, and σ_r, σ_z, σ_ϕ are the radial, axial, and circumferential stresses, respectively. τ_{rz} is the shear stress. The notation τ_{ij} is used to represent shear stresses where i denotes the direction of the stress component, while j denotes the surface on which the stress component acts. ε_r, ε_z, ε_ϕ, and γ_{rz} are the radial, axial, circumferential, and shear strains, respectively. Two boundary conditions were imposed, one for the outer domain boundary and one for the boundary between the scatterer and the surrounding medium (Fig. 1). A second-order nonreflecting boundary condition proposed by Bayliss–Gunzburger–Turkel (Bayliss *et al.*, 1982; Falou *et al.*, 2006b) was applied on the outer boundary. This boundary condition approximates an infinite space so that the scattered wave is not reflected back into the domain. The Bayliss–Gunzburger–Turkel condition is given by

$$\frac{\partial^2 p}{\partial r^2} + \left(\frac{4}{R_0} - 2ik\right)\frac{\partial p}{\partial r} + \left(\frac{2}{R_0} - 4ik\right)\frac{p}{R_0} - k^2 p = P_0 e^{-ikz}, \tag{7}$$

where k is the wave number ($k = \omega/c$) and R_0 is the radius of the boundary (which was three times that of the scatterer radius in this work). The term on the right-hand side represents the emitted plane wave from the transducer, P_0 (assumed to be 1 a.u.), whose direction is along the $+z$ axis. In the case of an elastic material immersed in a fluid, shear and surface waves may also exist inside and at the surface of the scatterer. The acoustic wave incident on the surface of the scatterer exerts a load on the surface of the elastic sphere described by

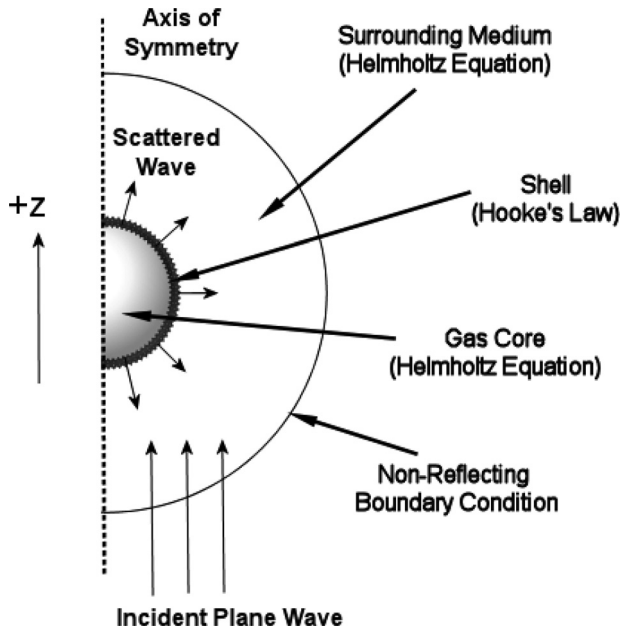

FIG. 1. Setup of the finite-element model for an UCA immersed in a fluid.

$$\mathbf{F} = -\mathbf{n}p, \tag{8}$$

where $\mathbf{F}$ is the face load, $\mathbf{n}$ is the outward pointing normal vector to the surface, and p the wave pressure on the surface (Ihlenburg, 1998; COMSOL, Inc., 2008). The normal component of acceleration was coupled at the surface of the scatterer in the solid (right-hand side) and fluid (left-hand side) domains,

$$\mathbf{n} \cdot \left(\frac{1}{\rho}\nabla p\right) = -(\mathbf{n} \cdot \mathbf{u})\omega^2, \tag{9}$$

where $\mathbf{u}$ is the time-harmonic displacement vector. COMSOL's implementation of the stress-strain formulation is based on the principle of virtual work, which states that for any displacement, the total work from internal strains is the negative of the work from external loads, so that their sum equals to zero (COMSOL, Inc., 2008; Oñate, 2009). Piecewise-linear polynomial on a grid of triangular elements also known as quadratic Lagrange triangular elements (Zienkiewicz *et al.*, 2005) were used in the discretization of the computational domain.

Among other solvers offered by the COMSOL multiphysics software package, the Unsymmetric-Pattern MultiFrontal Package or UMFPACK solver (Davis, 2004) was used to obtain a solution since it is fast (non-iterative). The finite-element model was executed on a computer having an Intel® Xeon™ 2.80 GHz Processor with 1 Gbyte of random access memory running Microsoft® Windows XP® operating system. The computation time was found to be 10 s per frequency on average.

B. UCA

UCAs are composed of an elastic shell encapsulating a gas core. The finite-element model (Fig. 1) described

previously had to be modified in such a way so that (a) the time-harmonic Helmholtz wave equation is used to model propagation of sound waves in the gas core as well as the domain outside the scatterer and (b) at the gas core-shell and shell-surrounding medium interfaces, both Eqs. (8) and (9) are imposed as boundary conditions to account for the presence of shear and surface waves inside and at the surface of the UCA shell. The number of mesh elements was chosen by studying the effect of refining the mesh on the backscatter pressure amplitude. It was found that 14 736 triangular elements are needed to obtain accurate solutions as shown in Fig. 2. Figure 3 illustrates the corresponding meshed model. The fundamental resonance frequency of a given UCA was found by determining the frequency that produces the first peak in its backscatter response. This frequency was compared to the analytical solution formulated by Church (1995). In his work, the UCA is modeled as a continuous layer of viscoelastic solid material (shell) that separates the gas core from the surrounding liquid and whose angular linear resonance frequency is given by

$$\omega_0 = \sqrt{(\rho_s R_{01}^2 \beta)^{-1}\left\{3\kappa P_h - \frac{2s_1}{R_{01}} - \frac{2s_2 R_{01}^3}{R_{02}^4} + 4\frac{V_s G_s}{R_{02}^3}\left[1 + S\left(1 + \frac{3R_{01}^3}{R_{02}^3}\right)\right]\right\}}, \tag{10}$$

where S is a term accounting for the strain, V_s is the volume, G_s is the shear modulus, ρ_s is the mass density, R_{01} is the inner radius, R_{02} is the outer radius, s_1 is the inner surface tension, and s_2 is the outer surface tension of the shell, respectively. P_h is the hydrostatic pressure (10^5 Pa), κ is the polytropic exponent (1.4 in the adiabatic case), and β is a term accounting for the difference in mass densities between the shell and the surrounding fluid. A 4 μm diameter perfluorocarbon phospholipid-coated contrast agent known as BR14 (Bracco Research SA, Geneva, Switzerland) surrounded by water was used to validate the finite-element model by comparing the resonance frequency predicted by both the finite-element model and the Church solution. This contrast agent was chosen since it is widely used and has been the subject of research by many investigators (Goertz *et al.*, 2003; Versluis *et al.*, 2004; Emmer *et al.*, 2007; Dollet *et al.*, 2008). Table I gives the physical properties of BR14 assumed to undergo adiabatic oscillations. The surface tensions at both the shell–gas and the shell–liquid interfaces were assumed to be negligible (Emmer *et al.*, 2007). A parametric study was also performed using the finite-element model to study the effects of changing the UCA parameters on its scattering behavior at high frequencies (1–70 MHz). The far-field scattered pressure from the UCA insonified by a plane wave traveling in the $+z$ direction was investigated by varying its diameter, shell thickness, and shell elasticity, while keeping other parameters fixed. It is believed that the finite-element model, which describes the basic fundamentals of sound wave propagation and stress–strain relationship within elastic material, may help in the understanding of the behavior of UCAs at high frequencies. It may also provide an insight into the presence of harmonic components in the UCA response observed experimentally at low pressures (Goertz *et al.*, 2005).

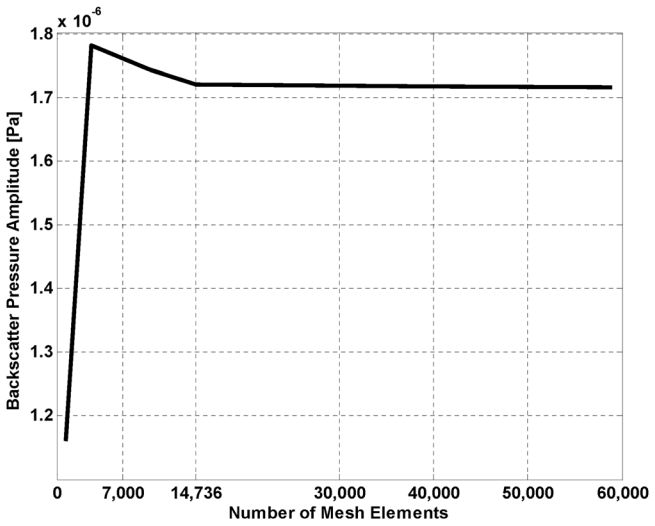

FIG. 2. Backscatter pressure amplitude (Pa) vs number of mesh elements.

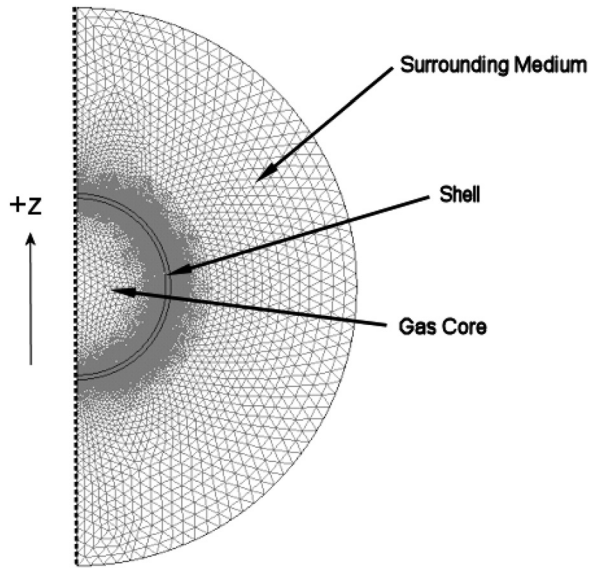

FIG. 3. Meshed model of UCA shown in Fig. 1. It is subdivided into 14 736 triangular elements.

TABLE I. Physical properties of the BR14 ultrasound contrast agent (Emmer *et al.*, 2007; Dollet *et al.*, 2008).

Property	Value
Shell thickness (δR_s)	3 nm
Shell density (ρ_s)	1100 kg/m^3
Shell's Young's modulus (E_s)	177.6 MPa
Shell's shear modulus (G_s)	60 MPa
Shell's Poisson's ratio (ν_s)	0.48
Perfluorocarbon density (ρ_g)	11.21 kg/m^3
Perfluorocarbon speed of sound (c_g)	100 m/s

III. RESULTS

We initially present the simulations results of a well calibrated microsphere suspended in water. Figure 4 shows the comparison between the analytical (Faran) and finite-element solutions for ultrasound scattering from a 30 μm polystyrene microsphere immersed in water. The plot shows the backscatter transfer function (BSTF) versus frequency. The maximum percentage error between both solutions was found to be less than 1%. Figure 5 depicts the deformations of the microsphere immersed in water at five resonance frequencies, which corresponded to surface modes (highlighted in Fig. 4). Figure 6 shows the angular distribution of scattering for the same microsphere at the first five resonance frequencies.

In order to validate the finite-element model results for UCAs, the resonance frequencies of the BR14 contrast agents having diameters ranging from 1 to 10 μm were compared against the Church model predictions. Figure 7 illustrates these comparisons. The maximum percentage error between the Church and the finite-element solutions was found to be less than 5%. The finite-element model was then used to examine how changes in the physical properties of the contrast agents would alter the scattering behavior and deformations of these agents as a function of frequency. Figure 8 shows the effects of varying the shell thickness from 3 to 100 nm on the backscatter response for a 4 μm BR14

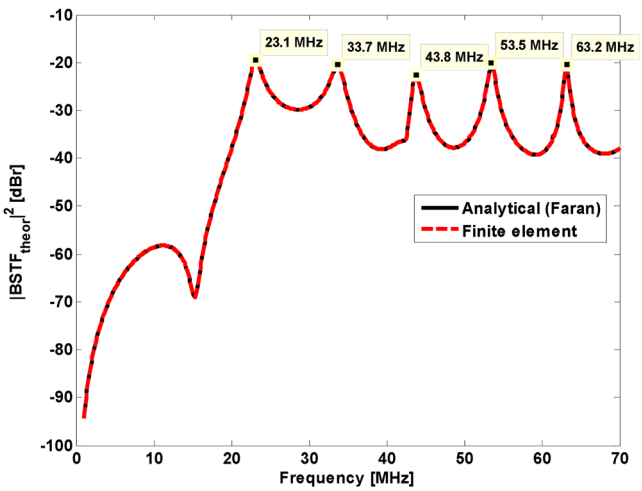

FIG. 4. (Color online) Analytical (Faran) and finite-element solutions for scattering from a 30 μm polystyrene microsphere immersed in water. The labels at the top denote the frequencies that produce peaks in the BSTF.

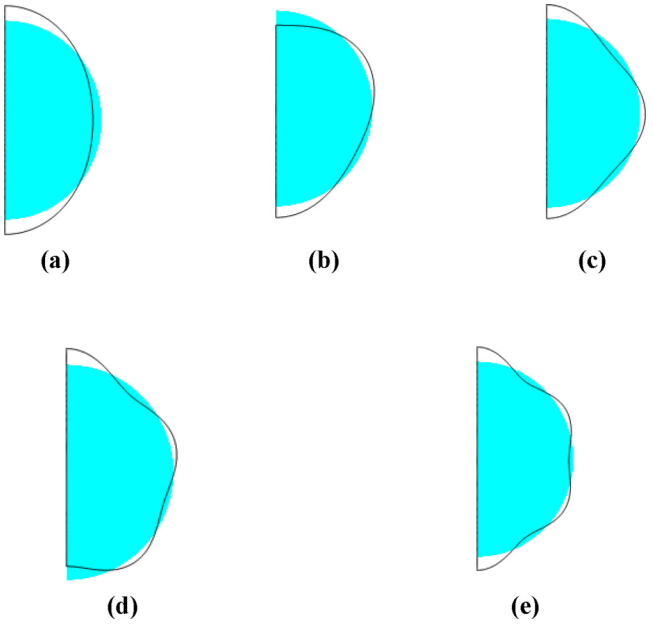

FIG. 5. (Color online) Finite-element solutions for deformations of a 30 μm polystyrene microsphere at (a) 23.1, (b) 33.7, (c) 43.8, (d) 53.5, and (e) 63.2 MHz. The plots show a snapshot of the maximum deformation for a slice parallel to the direction of wave propagation (bottom to top). The cyan half circle and the black curve illustrate the shape of the microsphere before and after applying the pressure, respectively. The displacement was multiplied by a factor of 4.5×10^7–1.6×10^8 for visualization purposes.

while keeping other parameters fixed. Figure 9 depicts the deformations of a 100 nm shelled UCA at five frequencies highlighted in Fig. 8. The angular distribution of scattered sound as a function of angle for the same UCA at five resonance frequencies is shown in Fig. 10. The effects of varying the shell shear modulus from 10 to 60 MPa on the backscatter response for a 100 nm shelled, 4 μm diameter UCA are shown in Fig. 11. Figure 12 shows the effects of varying the diameter from 1 to 6 μm on the backscatter response for a 100 nm shelled UCA. Figure 13 shows the relationship between shell thickness and monopole resonance frequency for a 4 μm UCA. Figure 14 shows the relationship between shell shear modulus and the resonance frequencies for a 100 nm, 4 μm UCA. The relationship between diameter and resonance frequencies for a 100 nm shelled UCA is shown in Fig. 15.

IV. DISCUSSION

Various analytical solutions have been developed by other investigators to study the behavior of scattering from spherical objects (Faran, 1951) and resonant scattering from UCAs (De Jong and Hoff, 1993; Church, 1995). While the Faran solution is based on the equation of wave propagation, predictions of resonances of UCAs are based on variants of the RP equation (such as the Church model) that describe the microbubble oscillation dynamics. These analytical solutions do not model wave propagation and the interactions of the pressure wave with the UCA shell. Therefore, most UCA models do not incorporate surface mode oscillations, which may lead to strong scattering at frequencies the Church model does not predict. Moreover, such analytical models

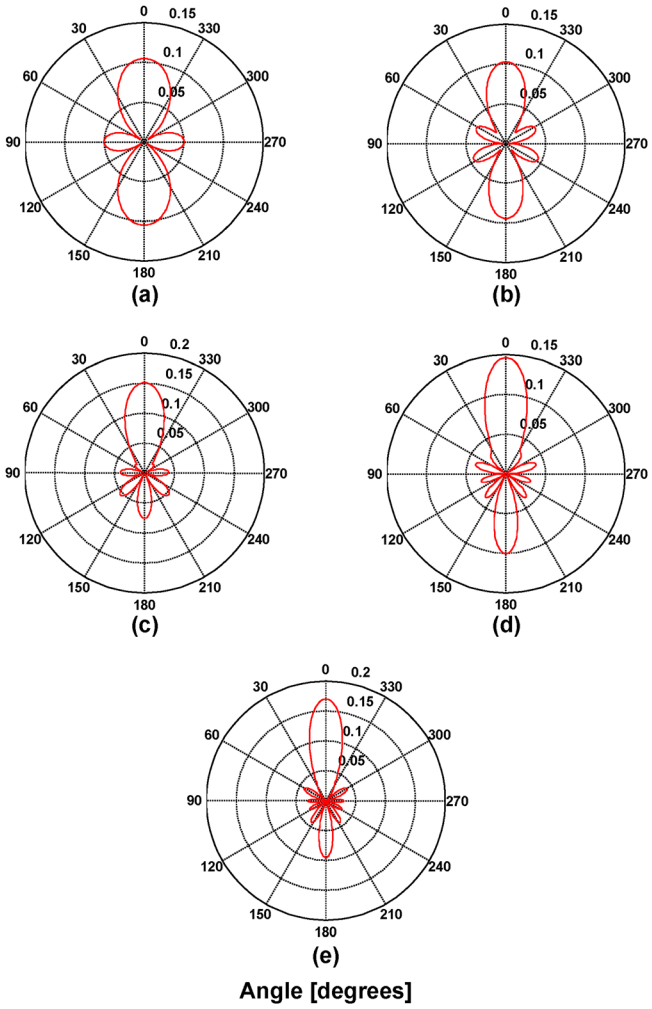

FIG. 6. (Color online) Finite-element solutions for angular scattering from a 30 μm polystyrene microsphere at (a) 23.1, (b) 33.7, (c) 43.8, (d) 53.5, and (e) 63.2 MHz. The plots show the pressure amplitude (Pa) vs angle (deg). Backscattering occurs at 180°.

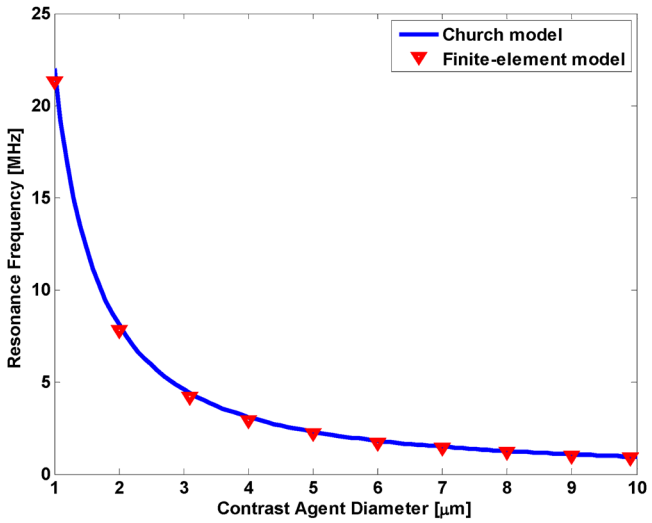

FIG. 7. (Color online) Resonance frequency vs contrast agent diameter: Comparison between the Church (solid line) and finite-element (inverted triangles) solutions.

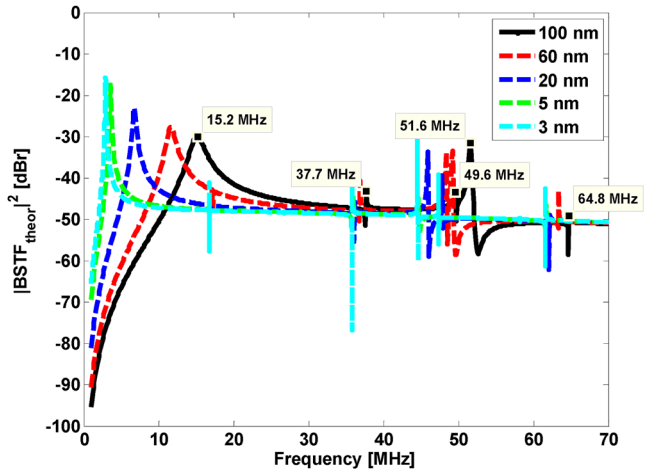

FIG. 8. (Color online) Effects of varying the shell thickness on the backscatter response for 4 μm diameter BR14 contrast agent. The labels at the top denote the frequencies that produce peaks in the BSTF for the 100 nm shelled UCA.

cannot take into account shell defects (Bloch *et al.*, 2004; Kooiman *et al.*, 2010) or time-varying properties (Borden *et al.*, 2005). A finite-element model that can incorporate such complexities was developed and validated by comparing the finite-element model solution of wave propagation to the Faran analytical solution for a 30 μm polystyrene microsphere. It was then applied to shelled objects such as UCAs.

A. Polystyrene microsphere

An excellent agreement was found between the analytical and finite-element solutions, despite the large changes in pressure as a function of ultrasound frequency as shown in

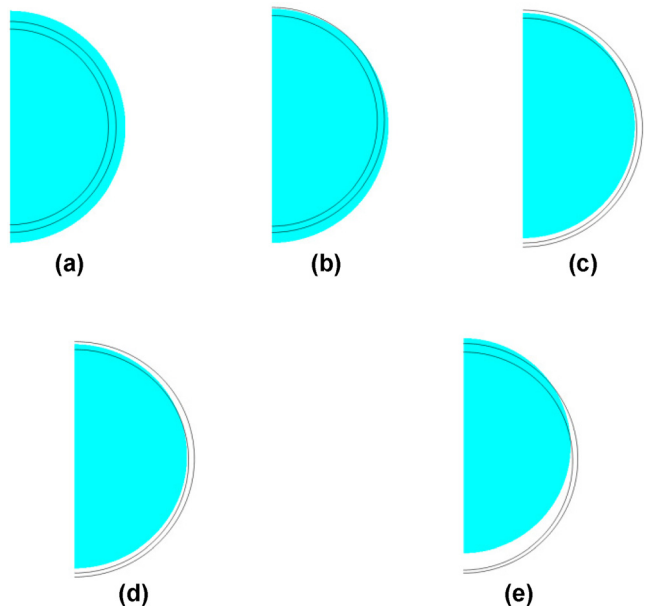

FIG. 9. (Color online) Finite-element solutions for deformations of a 100 nm shelled, 4 μm diameter UCA at (a) 15.2, (b) 37.7, (c) 49.6, (d) 51.6, and (e) 64.8 MHz. The plots show a snapshot of the maximum deformation for a slice parallel to the direction of wave propagation (bottom to top). The cyan half circle and the black curve illustrate the shape of the UCA before and after applying the pressure, respectively. The displacement was multiplied by a factor of 3.5×10^5–5×10^7 for visualization purposes.

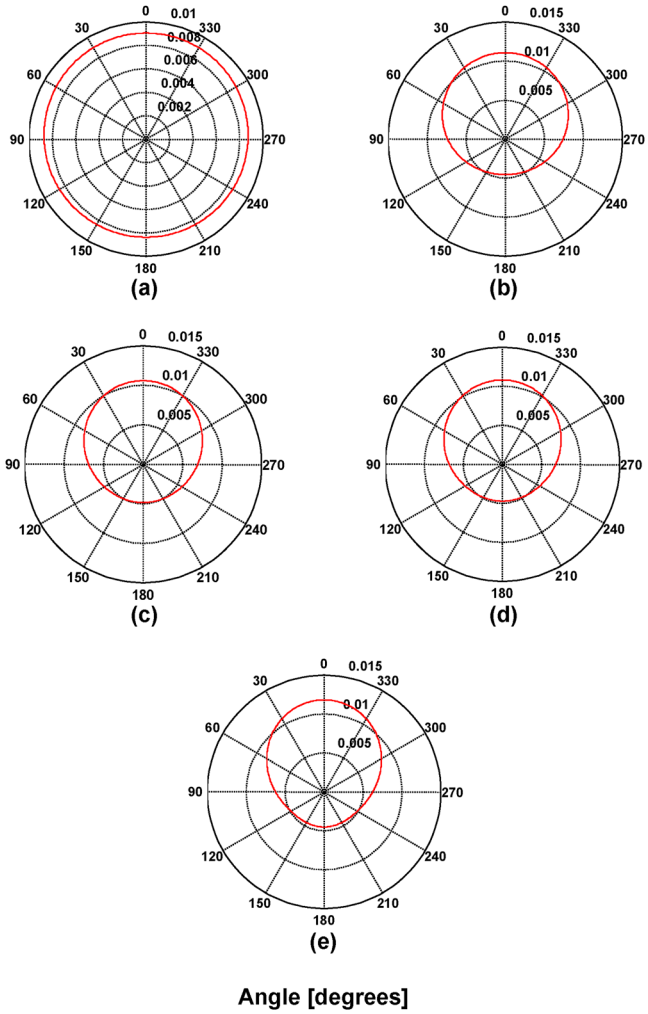

FIG. 10. (Color online) Finite-element solutions for angular scattering from a 100 nm shelled, 4 μm diameter UCA at (a) 15.2, (b) 37.7, (c) 49.6, (d) 51.6, and (e) 64.8 MHz. The plots show the pressure amplitude (Pa) vs angle (deg). Backscattering occurs at 180°.

Fig. 4. Various wide peaks of comparable magnitudes were found in the backscatter of the microsphere and correspond to its resonance frequencies. The first five resonances occur at 23.1, 33.7, 43.8, 53.5, and 63.2 MHz. A close look at the

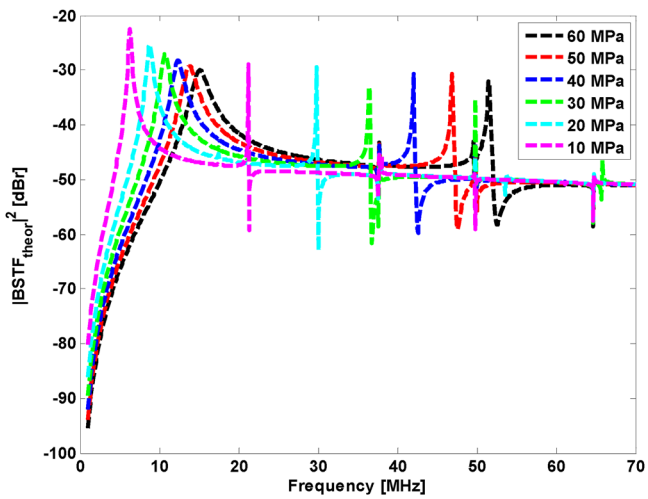

FIG. 11. (Color online) Effects of varying the shell shear modulus on the backscatter response for a 100 nm shelled, 4 μm diameter UCA.

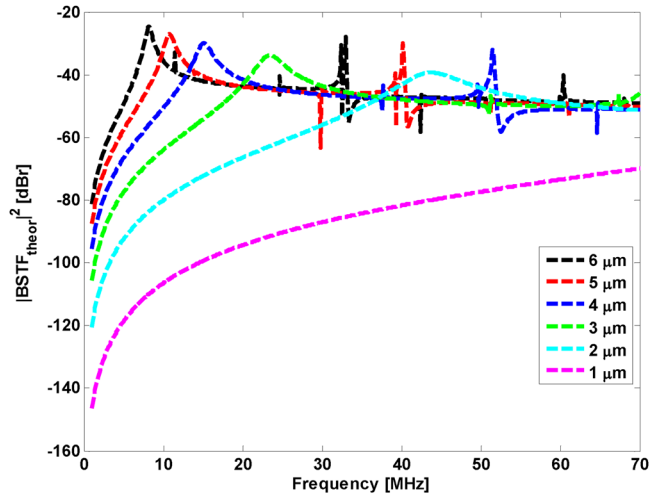

FIG. 12. (Color online) Effects of varying the contrast agent's diameter on the backscatter response for a 100 nm shelled UCA.

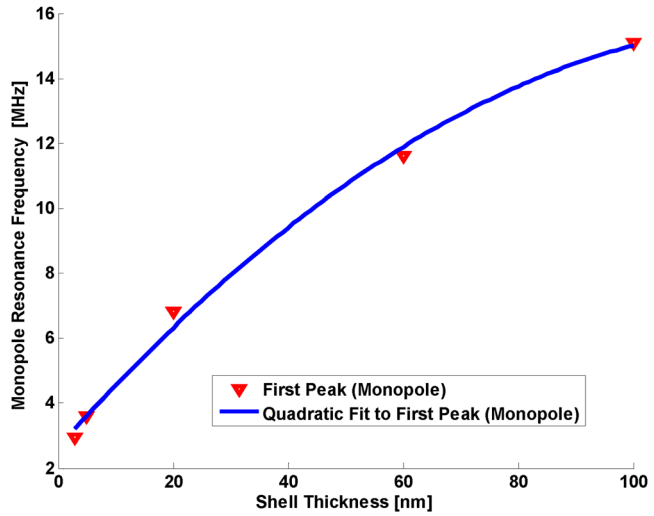

FIG. 13. (Color online) Relationship between shell thickness and monopole resonance frequency for a 4 μm UCA.

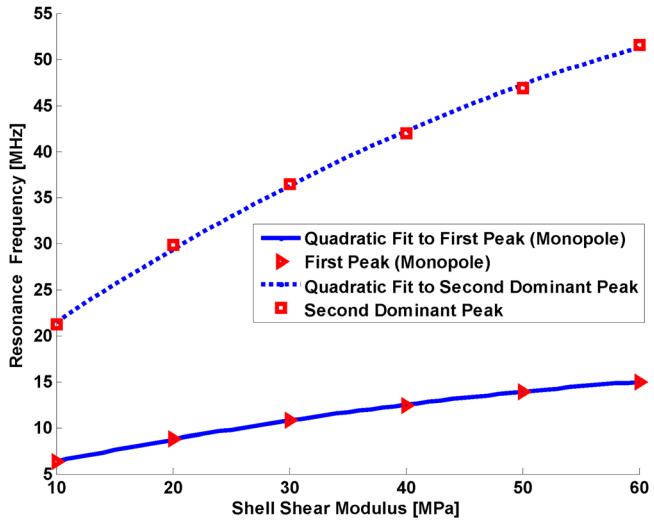

FIG. 14. (Color online) Relationship between shell shear modulus and the resonance frequencies for a 100 nm, 4 μm UCA.

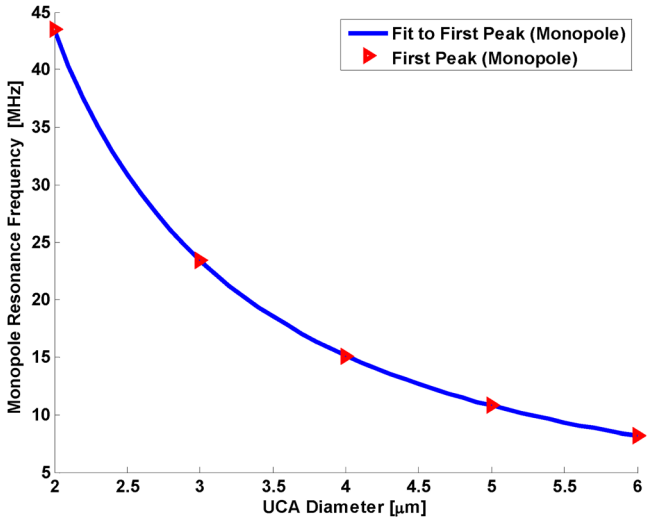

FIG. 15. (Color online) Relationship between diameter and monopole resonance frequency for a 100 nm shelled UCA.

deformations of the polystyrene microsphere at its resonance frequencies (Fig. 5) reveals the presence of non-spherical oscillations, or surface modes, at these frequencies which become more complex in shape as the frequency increases. At 23.1 MHz (lowest resonance frequency), the microsphere oscillates between a prolate and oblate spheroidal shape, known as quadrupole mode or mode $n=2$ (Uberall *et al.*, 1996). The octupole mode ($n=3$) occurs at 33.7 MHz, where three wavelengths of the surface distortion are needed to span the microsphere's circumference. Four ($n=4$), five ($n=5$), and six ($n=6$) wavelengths of the surface distortion are required to span the microsphere's circumference at 43.8, 53.5, and 63.2 MHz, respectively. The angular distribution of scattering becomes more complex in shape as the frequency increases (Fig. 6). A distinct angular directivity characterizes each resonance frequency because of multipole effects. The forward- and backscattering amplitudes are identical at 23.1 and 33.7 MHz ($n=2$, 3). For frequencies above 33.7 MHz, the forward scattering becomes stronger than the backscatter. The number of scattering lobes also increases as a function of the resonance frequency, which is likely related to the multipole effects. No monople or dipole modes ($n=0$, 1) were found at resonances in the frequency range of interest.

B. BR14 UCA

A very good agreement (maximum error of $<5\%$) was found between the finite-element model and the Church analytical solution (Fig. 7). The monopole resonance frequency decreases with the increase of the contrast agent diameter, which agrees with previous findings (De Jong and Hoff, 1993; Church, 1995). Increasing the shell thickness of the UCA produces new features in the backscatter response as shown in Fig. 8. When the shell thickness is increased from 3 to 100 nm, with the other simulation parameters held constant, several changes in the ultrasound backscatter power occur. The monopole peak became wider, decreased in height, and increased to 15.2 MHz from 2.9 MHz with the increase of shell thickness. For 100 nm thick shelled contrast agent, four other peaks appear at 37.7, 49.6, 51.6, and 64.8 MHz. The peak centered at 51.6 MHz is of a comparable height to that of the monopole peak at 15.2 MHz. A study of the deformations of this UCA leads to some interesting findings. First, at 15.2 MHz, the UCA contracts and expands periodically and exhibits the breathing mode or $n=0$. At higher resonance frequencies, the UCA undergoes a shape deformation characterized by a translational motion, in addition to contraction and expansion. The UCA shell thickness becomes non-uniform as the UCA oscillates: Thinning of the shell occurs in the direction of the translation, whereas thickening occurs in the opposite direction as shown in Figs. 9(d) and 9(e). This change in shell thickness is particularly seen at high resonance frequencies (51.6 and 64.8 MHz). The surface modes illustrated in Fig. 9 seem to correlate with the angular scattering shown in Fig. 10. For the monopole resonance at 15.2 MHz, an isotropic scattering is obtained, which is similar to that of a free air bubble (Falou *et al.*, 2006a). At higher resonance frequencies (37.7, 49.6, 51.6, 64.8 MHz), the scattering amplitude is directional and is of greater magnitude in the forward direction compared to the back direction. This is likely due to the translational motion of the contrast agent observed at these frequencies. The shape oscillations of the contrast agent above the monopole resonance appear to be the result of the summation of various surface modes. The resonance peaks at 49.6, 51.6, and 64.8 MHz are identified as overtones of the resonance peak at 37.7 MHz since they all exhibit similar shape oscillations and angular distributions of scattering. It is instructive to compare the surface modes exhibited by the UCA to those exhibited by the polystyrene microsphere. The former developed a breathing mode ($n=0$) at the fundamental resonance frequency and a collection of complex oscillations at higher frequencies, in contrast to the latter, which does not exhibit the breathing mode but rather higher modes starting with $n=2$ (quadrupole mode) and ending with mode $n=6$ for the range of frequencies studied. For the polystyrene microsphere, a systematic relationship exists between the resonance frequency and its corresponding surface mode. The higher the resonance frequency, the more complex the oscillation pattern, and hence the higher is the mode number. No such relationship was found for the UCA.

The study of surface modes of microspheres and UCAs in particular may have implications on imaging and therapeutic applications. Surface modes may play a role in the generation of the acoustical energy during harmonic imaging with UCAs, a promising imaging technique that offers a very good contrast between tissue and blood vasculature (Goertz *et al.*, 2007; Jafari Sojahrood *et al.*, 2011). They may also provide insights into the shell properties, which may lead to a better modeling of the shell behavior. In terms of therapeutic applications, surface modes will help in the understanding of the mechanism of microbubble rupture and the release of drug during localized drug delivery process, as stress/strain distributions in the shell can be studied in detail.

As discussed earlier, when the shell thickness is increased, the monopole peak becomes wider, decreases in height, and shifts toward higher frequencies. An empirical

quadratic relationship was found between the shell thickness and the monopole resonance frequency as shown in Fig. 13. Increasing the shell's shear modulus from 10 to 60 MPa for the 100 nm shelled UCA, while keeping other parameters fixed (Fig. 11), produced similar effects to those obtained as the result of the increase in the shell thickness. The monopole and the second dominant (whose magnitude is comparable to that of the monopole) backscatter peaks in the range of frequencies studied became wider and shifted to higher frequencies. For the 10 MPa shell, these peaks were initially centered at 6.3 and 21.2 MHz, and with increasing shear modulus, they shifted to 15.2 and 51.6 MHz for the 60 MPa shell, respectively. In addition, the difference between the frequencies of the monopole and the second dominant peaks increases as the shell's shear modulus increases (6.3 and 21.2 MHz for 10 MPa vs 15.2 and 51.6 MHz for 60 MPa). A quadratic relationship was also found between the shell's shear modulus and the monopole and second dominant resonance frequencies as shown in Fig. 14. When the diameter of a 100 nm shell UCA is decreased from 6 to 1 μm, with the other simulation parameters held constant, several features changed in the backscatter response. The monopole peak became wider, decreased in height, and shifted toward higher frequencies. High resonant peaks originally presented in the backscatter of UCAs whose diameters are larger than 3 μm are no longer present in the backscatter of UCAs of smaller diameters. The monopole resonance peak is not visible for the 1 μm UCA and likely occurred at a frequency outside the range of this study. The UCA monopole resonance frequency varies as a function of the inverse of the square root of the UCA diameter cubed (volume) as shown in Fig. 15.

The results reported in this work show that the shell thickness, its elasticity, and the diameter of the UCA play a significant role in the generation of other resonance peaks at high frequencies, which may contribute to the generation of harmonics (useful for imaging) and stresses that may lead to UCA collapse (useful for therapy). This may provide an explanation for the presence of harmonics in the backscatter of the Definity UCA (Goertz *et al.*, 2005). This study also shows that more careful design approaches may be taken to maximize the backscatter response from UCAs for imaging purposes. This can be achieved by using the developed finite-element model, which describes the basic fundamentals of sound wave propagation and stress–strain relationship within the elastic material, to optimize the UCA parameters in order to obtain the desired results. It also shows that a relationship exists between resonance frequencies and surface modes. This is particularly important for the understanding of the mechanism of drug release from drug delivery vehicles (such as drug encapsulated polymer microspheres) for therapeutic applications. The number of fragments formed during the UCA fragmentation has been linked to surface modes (Versluis *et al.*, 2004) and hence a study of these modes will help in determining the optimal conditions for the drug release.

In the current model, the Helmholtz wave equation was used to solve wave propagation in the surrounding medium. It does not take into account dissipative effects in the liquid which could lead to signal loss due to attenuation. Previous investigators (Baddour *et al.*, 2005; Falou *et al.*, 2010) have shown that this assumption is valid for single scatterers suspended in water where a very good agreement was found between analytical solutions (which were shown to be identical to finite-element computations in this work as shown in Fig. 4) and experimental measurements. In surrounding media with high attenuation, such losses can be incorporated into the model by the addition of a complex expression for the wave number in the Helmholtz equation. In addition, the current model does not account for non-linearity associated with wave propagation in biological media. This will be incorporated in future models.

V. CONCLUDING REMARKS

A finite-element model, built upon the fundamentals of acoustics and structural mechanics, was introduced to study the dynamic behavior and the backscatter responses of elastic microspheres and UCAs. An excellent agreement was found between the analytical and finite-element solutions for the backscatter from individual polystyrene microspheres and predictions of the resonance frequencies of UCAs. For the polystyrene microspheres, a systematic relationship was found between the resonance frequencies and the microsphere surface modes, which appear in the form of nonspherical deformations. A correlation was also found between the resonance frequency and the angular distribution of scattering, which becomes more complex in shape as the frequency increases. On the other hand, for the UCA, no systematic relationship between the resonance frequencies and the surface modes was found. Instead, the UCA exhibited a collection of complex oscillations, which appear to be a combination of various surface modes. This was also confirmed by examining the angular distribution of scattering at its resonance frequencies. A study of the effects of varying the shell properties on the resonance frequencies of UCAs provided some insights into their backscatter behaviors, which could be exploited for imaging purposes. The finite-element model developed in this work was shown to provide a better framework for understanding the scattering and the shape oscillations of spherical objects such as microspheres and UCAs.

Future work includes the experimental measurement of the backscatter response from individual UCAs (Falou *et al.*, 2010) which could be compared to theoretical predictions of the finite-element model. If required, non-linear wave propagation in the surrounding medium and heterogeneity within the UCA shell (Kooiman *et al.*, 2010) will be incorporated into the finite-element model. Parametric studies will be conducted to estimate some of the UCAs' physical properties (such as the shell's elasticity) that are hard to measure experimentally. Once this has been accomplished, the finite-element model will be used to understand the scattering behavior of targeted UCAs when they are bound to cells or inhibited from oscillating freely due to other obstacles. Such understanding is crucial for various targeted ultrasound imaging applications, such as molecular imaging.

ACKNOWLEDGMENTS

The authors acknowledge the COMSOL, Inc. (Burlington, MA) support team members for their technical support. This work was supported by operating grants from the Canadian Institutes of Health Research (Grant Nos. MOP-97959 and 79447), and Canada Research Chairs Program awarded to M.C.K, and Ryerson University. O.F. has been supported by the Ontario Graduate Scholarship (OGS) and the Graduate Research Excellence Award awarded by Ryerson University.

Allen, J. S., Kruse, D. E., and Ferrara, K. W. (**2001**). "Shell waves and acoustic scattering from ultrasound contrast agents," IEEE Trans. Ultrason. Ferroelectr. Freq. Control **48**, 409–418.

Baddour, R. E., Sherar, M. D., Hunt, J. W., Czarnota, G. J., and Kolios, M. C. (**2005**). "High- frequency ultrasound scattering from microspheres and single cells," J. Acoust. Soc. Am. **117**, 934–943.

Bayliss, A., Gunzburger, M., and Turkel, E. (**1982**). "Boundary-conditions for the numerical-solution of elliptic-equations in exterior regions," SIAM J. Appl. Math. **42**, 430–451.

Bloch, S. H., Wan, M., Dayton, P. A., and Ferrara, K. W. (**2004**). "Optical observation of lipid- and polymer-shelled ultrasound microbubble contrast agents," Appl. Phys. Lett. **84**, 631–633.

Borden, M. A., Kruse, D. E., Caskey, C. F., Zhao, S., Dayton, P. A., and Ferrara, K. W. (**2005**). "Influence of lipid shell physicochemical properties on ultrasound-induced microbubble destruction," IEEE Trans. Ultrason. Ferroelectr. Freq. Control **52**, 1992–2002.

Calliada, F., Campani, R., Bottinelli, O., Bozzini, A., and Sommaruga, M. G. (**1998**). "Ultrasound contrast agents: Basic principles," Eur. J. Radiol. **27**, S157–S160.

Church, C. C. (**1995**). "The effects of an elastic solid-surface layer on the radial pulsations of gas-bubbles," J. Acoust. Soc. Am. **97**, 1510–1521.

COMSOL, Inc. (**2008**). *Acoustics Module: User's Guide* (COMSOL, Inc., Burlington, MA).

Davis, T. A. (**2004**). "Algorithm 832: Umfpack v4.3—An unsymmetric-pattern multifrontal method," ACM Trans. Math. Softw. **30**, 196–199.

De Jong, N., and Hoff, L. (**1993**). "Ultrasound scattering properties of albunex microspheres," Ultrasonics **31**, 175–181.

Demkowicz, L., and Shen, J. (**2006**). "A few new (?) facts about infinite elements," Comput. Methods Appl. Mech. Eng. **195**, 3572–3590.

Deng, C. X., Lizzi, F. L., Silverman, R. H., Ursea, R., and Coleman, D. J. (**1998**). "Imaging and spectrum analysis of contrast agents in the in vivo rabbit eye using very-high-frequency ultrasound," Ultrasound Med. Biol. **24**, 383–394.

Doinikov, A. A., and Dayton, P. A. (**2007**). "Maxwell rheological model for lipid-shelled ultrasound microbubble contrast agents," J. Acoust. Soc. Am. **121**, 3331–3340.

Dollet, B., van der Meer, S. M., Garbin, V., de Jong, N., Lohse, D., and Versluis, M. (**2008**). "Nonspherical oscillations of ultrasound contrast agent microbubbles," Ultrasound Med. Biol. **34**, 1465–1473.

Eaton, J. A., and Regan, B. A. (**1996**). "Application of the finite element method to acoustic scattering problems," AIAA J. **34**, 29–34.

Emmer, M., van Wamel, A., Goertz, D. E., and de Jong, N. (**2007**). "The onset of microbubble vibration," Ultrasound Med. Biol. **33**, 941–949.

Everstine, G. C., and Henderson, F. M. (**1990**). "Coupled finite-element boundary element approach for fluid structure interaction," J. Acoust. Soc. Am. **87**, 1938–1947.

Falou, O., Kumaradas, J. C., and Kolios, M. C. (**2005**). "A study of femlab for modeling high frequency ultrasound scattering by spherical objects," *Proceedings of FEMLAB Users Conference,* Boston, MA (October 23–25, 2006).

Falou, O., Kumaradas, J. C., and Kolios, M. C. (**2006a**). "Finite element modeling of ultrasound scattering by spherical objects and cells," *Proc.-IEEE Ultrason. Symp*., Vancouver, Canada (October 2–6, 2006), pp. 2072–2075.

Falou, O., Kumaradas, J. C., and Kolios, M. C. (**2006b**). "Modeling acoustic wave scattering from cells and microbubbles," *Proceedings of COMSOL Users Conference*, Boston, MA (October 22–24, 2006).

Falou, O., Rui, M., El Kaffas, A., Kumaradas, J. C., and Kolios, M. C. (**2010**). "The measurement of ultrasound scattering from individual micron-sized objects and its application in single cell scattering," J. Acoust. Soc. Am. **128**, 894–902.

Faran, J. J. (**1951**). "Sound scattering by solid cylinders and spheres," J. Acoust. Soc. Am. **23**, 405–418.

Goertz, D. E., Cherin, E., Needles, A., Karshafian, R., Brown, A. S., Burns, P. N., and Foster, F. S. (**2005**). "High frequency nonlinear b-scan imaging of microbubble contrast agents," IEEE Trans. Ultrason. Ferroelectr. Freq. Control **52**, 65–79.

Goertz, D. E., Frijlink, M., Bouakaz, A., Chin, C. T., De Jong, N., and Van Der Steen, A. W. F. (**2003**). "The effect of bubble size on nonlinear scattering from microbubbles at high frequencies," Proc.-IEEE Ultrason. Symp. **2**, 1503–1506.

Goertz, D. E., Frijlink, M. E., Tempel, D., Bhagwandas, V., Gisolf, A., Krams, R., de Jong, N., and van der Steen, A. F. W. (**2007**). "Subharmonic contrast intravascular ultrasound for vasa vasorum imaging," Ultrasound Med. Biol. **33**, 1859–1872.

Greis, C. (**2011**). "Quantitative evaluation of microvascular blood flow by contrast-enhanced ultrasound (ceus)," Clin. Hemorheol. Microcirc. **49**, 137–149.

Hunt, J. T., Knittel, M. R., Nichols, C. S., and Barach, D. (**1975**). "Finite-element approach to acoustic scattering from elastic structures," J. Acoust. Soc. Am. **57**, 287–299.

Ihlenburg, F. (**1998**). *Finite Element Analysis of Acoustic Scattering* (Springer, New York).

Jafari Sojahrood, A., Gong, Y., Falou, O., Porter, T., and Kolios, M. C. (**2011**). "Dynamics of ultrasound contrast agents at high multiples of their resonance frequency and their clinical relevance," *Proceedings of American Institute of Ultrasound in Medicine Annual Convention*, New York (April 14–17, 2011), p. S71.

Ketterling, J. A., Mamou, J., Allen, J. S., Aristizabal, O., Williamson, R. G., and Turnbull, D. H. (**2007**). "Excitation of polymer-shelled contrast agents with high-frequency ultrasound," J. Acoust. Soc. Am. **121**, EL48–EL53.

Kooiman, K., Emmer, M., Kokhuis, T. J. A., Bosch, J. G., de Gruiter, H. M., van Royen, M. E., van Cappellen, W. A., Houtsmuller, A. B., van der Steen, A. F. W., and de Jong, N. (**2010**). "Lipid distribution and viscosity of coated microbubbles," *Proc.-IEEE Ultrason. Symp*., San Diego, CA (October 11–14, 2010) 900–903.

Leighton, T. G. (**2004**). *The Acoustic Bubble* (Academic, London), chap. 4.

Logan, D. L. (**2012**). *A First Course in Finite Element Method* (Cengage Learning, Stamford, CT), Chap. 9.

Moran, C. M., Watson, R. J., Fox, K. A. A., and McDicken, W. N. (**2002**). "In vitro acoustic characterisation of four intravenous ultrasonic contrast agents at 30 mhz," Ultrasound Med. Biol. **28**, 785–791.

Numrich, S. K., Varadan, V. V., and Varadan, V. K. (**1981**). "Scattering of acoustic-waves by a finite elastic cylinder immersed in water," J. Acoust. Soc. Am. **70**, 1407–1411.

Oñate, E. (**2009**). *Structural Analysis with the Finite Element Method. Linear Statics* (Springer, Barcelona, Spain), chap. 7.

Pauzin, M. C., Mensah, S., and Lefebvre, J. P. (**2007**). "Development of a finite element model of ultrasound contrast agent," *Proc.-IEEE Ultrason. Symp*., New York (October 28–31, 2007) 1989–1992.

Stride, E., and Saffari, N. (**2003**). "Microbubble ultrasound contrast agents: A review," Proc. Inst. Mech. Eng., Part H: J. Eng. Med. **217**, 429–447.

Uberall, H., Ripoche, J., Maze, G., and Izbicki, J.-L. (**1996**). "The resonances: From nuclear physics to underwater acoustics," in *Acoustic Interactions with Submerged Elastic Structures*, edited by A. Guran, J. Ripoche, and F. Ziegler (World Scientific, River Edge, NJ), pp. 1–14.

Versluis, M., Van Der Meer, S. M., Lohse, D., Palanchon, P., Goertz, D., Chin, C. T., and De Jong, N. (**2004**). "Microbubble surface modes," Proc.-IEEE Ultrason. Symp. **1**, 207–209.

Wilton, D. T. (**1978**). "Acoustic radiation and scattering from elastic structures," Int. J. Numer. Methods Eng. **13**, 123–138.

Zienkiewicz, O. C., Taylor, R. L., and Zhu, J. Z. (**2005**). *The Finite Element Method: Its Basis and Fundamentals* (Elsevier Butterworth-Heinemann, Oxford, UK), Chap. 4.